Improving NV centre density during diamond growth by CVD process using N2O gas

Midrel Wilfried Ngandeu Ngambou, Clément Pellet-Mary, Ovidiu Brinza, Alessi Antonino, Gabriel Hetet, Alexandre Tallaire, Fabien Bénédic, Jocelyn Achard

Improving NV centre density during diamond growth by CVD process using N_2O gas

Midrel Wilfried Ngandeu Ngambou[1], Clément Pellet-Mary[2], Ovidiu Brinza[1], Alessi Antonino[3], Gabriel Hetet[2], Alexandre Tallaire[4], Fabien Bénédic[1], Jocelyn Achard[1]

[1] *LSPM-CNRS, Université Sorbonne Paris Nord, 93430 Villetaneuse, France*

[2] *LPENS-CNRS, Ecole Normale Supérieure, PSL Research University, 75231 Paris, France*

[3] *Laboratoire des Solides Irradiés UMR 7642 CEA – CNRS – Ecole polytechnique, Route de Saclay, 91128 PALAISEAU Cedex, France*

[4] *IRCP-CNRS, Chimie ParisTech, PSL Research University, 75005, Paris, France*

Abstract:

Nitrogen-Vacancy (NV) centres in diamond are point-like defects that have attracted a lot of attention as promising candidates for quantum technologies particularly for sensing and imaging nanoscale magnetic fields. For this application, the use of a high NV density within a high-quality diamond layer is of prime interest. In previous works, it has been demonstrated that in situ doping with N_2O rather than N_2 during Chemical Vapour deposition (CVD), limits the formation of macroscopic defects and improves NV's photostability. In this work, we focus on the optimization of the CVD growth conditions to obtain a high NV density keeping a constant N_2O concentration in the gas phase (100 ppm). For this purpose, freestanding CVD layers are prepared varying two main growth parameters: methane content and substrate temperature. High energy electron irradiation followed by annealing is finally carried out in order to increase the NV yield through partial conversion of N impurities. Defect concentrations and spin properties are investigated. We find that growth under lower methane concentrations and lower temperatures enhances NV doping. NV ensembles with a density of the order of 2 ppm are finally obtained with narrow spin resonance linewidth. In addition, higher annealing temperatures of 1200°C following irradiation are found to efficiently remove defects thus improving spin properties.

Keywords: Quantum technologies; Single Crystal diamond; NV centres; Chemical vapour deposition; Defects

1. Introduction

During the last decade, the NV centre has become one of the most studied colour centres in diamond. It is a stable lattice defect consisting of a nitrogen atom, a common impurity in diamond that can be found as a single substitutional defect and a vacancy. Once isolated by optical confocal microscopy at the individual level, its photoluminescence is very strong and stable. This defect has two possible charge states: the neutral state (NV^0) and the negatively charged state (NV^-). Only the latter has an electronic spin structure that can be detected as an individual quantum system, prepared in a defined quantum state by optical pumping, and then coherently manipulated using microwave fields. Interestingly, the NV centre retains its coherent state for a relatively long duration of up to several ms in isotopically purified crystals even at room temperature [1]. This set of unique characteristics for a solid-state defect has led to a wide range of applications: magnetic sensing [2–5], quantum cryptography [6,7], single photon sources [8–10], luminescent diamond nanoparticles for drug delivery in cells [11], spin-based qubits for quantum information processing [12,13] etc. However, these applications require having an accurate control of NV properties, in particular in terms of density, environment and spatial localization.

NV centres can be created either by nitrogen (N^+) ion implantation [14,15] generally followed by a post processing annealing [16] or by in situ doping using nitrogen gas precursor during diamond deposition [17–19]. The latter approach usually leads to longer coherence times although spatial localization at the surface or in-depth is more difficult to achieve. The synthesis of diamonds containing a large amount of NV centres (> 1 ppm) is also desirable to improve the sensitivity of quantum sensors but is hampered by a poor N solubility in diamond and a low NV creation yield with respect to substitutional nitrogen. The use of irradiation treatments, in general with high energy electrons, provides a way to increase NV concentration in either implanted or as-grown diamond films by generating the required vacancies to convert part of the nitrogen into NVs. Using such post-treatments, NV creation yield can reach up to 20 % [20].

In this paper, we relied on in situ doping using a non-conventional gas precursor (N_2O) to generate dense ensembles of NV centres in bulk diamond crystals prepared by Plasma Assisted Chemical Vapour Deposition (PACVD). Indeed, N_2 as a doping gas suffers from low doping efficiencies and, at high concentration, leads to growth defects [21], unlike N_2O that is well adapted to obtain high NV densities with good optical properties even when hundreds of ppm

of this gas are introduced [20]. The main advantage of N_2O is related to the lower bond dissociation energy of N-O (197.6 kJ/mol) than O=O (490.4 kJ/mol) [22] leading to an easier production of O-radicals in the plasma for the growth of CVD diamond and thereby improving crystalline quality [23]. Moreover, from a practical point of view, the use of only one gas precursor for adding both nitrogen and oxygen eases the implementation and the control of the process. In addition to the in-situ doping, which has a typical NV creation yield of less than 1 %, we used electron irradiation at high energy (2.3 MeV) followed by thermal annealing to create and diffuse vacancies towards substitutional nitrogen impurities.

In order to elucidate the CVD growth conditions that are more favourable to create bulk crystals with dense NV ensembles, we prepared several thick diamond films under varying input process parameters such as substrate temperature and methane concentration before using a post-treatment by electron irradiation. We eventually assessed the density and spin properties of the NV centres using a wide range of experimental techniques. In particular, we focused on the $[NV^-]/ [NV_{Total}]$ ratio which must be maximized since only the negatively charge state of this defect possesses adequate properties for quantum sensing (where $[NV_{Total}]$ is the sum of $[NV^0]$ and $[NV^-]$). We observed that growth under lower methane concentrations and lower temperatures enhances doping and promotes negatively charged NV centres. In addition, higher annealing temperatures of 1200 °C are found to efficiently remove defects generated by irradiation, such as VH^-, and lead to improved Electron Spin Resonance (ESR) linewidths.

2. Experimental details

Four thick nitrogen-doped CVD layers were grown on type *Ib* High Pressure High Temperature (HPHT) (100)-oriented single crystal diamond substrates by PACVD [24] using a N_2O concentration of 100 ppm in the gas phase. During growth, the total gas pressure and input microwave power were maintained constant at 200 mbar and 3000 W, respectively. The total gas flow injected in the reactor was 500 sccm. The growth conditions under which these samples were obtained are summarized in **Table 1**. The only parameters that were modified are substrate temperature and methane concentration which have been varied from 850 °C to 1000 °C and from 3 % to 7 %, respectively. The evolution of the growth rate as a function of methane concentration and temperature (last column of Table 1) is already described in the literature by several groups working on single crystal diamond growth [24]. After growth, the samples were laser cut and polished to produce freestanding CVD plates with thicknesses in the range of 160-

350 µm allowing optical transmission characterizations. Based on our previous investigation, we expect the total nitrogen concentration in the CVD films to be in the range 10 to 30 ppm [25].

Samples	Substrate temperature (°C)	Methane concentration (%)	Growth thickness (µm)	Growth rate (µm/h)
A	850	4	270	41
B	1000	4	297	38
C	1000	3	166	19
D	1000	7	340	68

Table 1: Growth conditions, resulting thicknesses and growth rate of the synthetized films. The parameter that was specifically varied is highlighted in grey.

After growth, in order to improve NV density, a post-treatment consisting of electron irradiation at an energy of 2.3 MeV was performed at room temperature using the electron accelerator platform SIRIUS located at LSI laboratory [26]. A dose of 3×10^{18} electrons.cm^{-2} was used to produce a vacancy density of the order of magnitude of the expected N concentration. Indeed, in this energy range around 0.7 vacancies are produced for each electron [27]. Following the irradiation step, an annealing at 800°C during 2 hours under secondary vacuum in the range 4 to 8×10^{-5} mbar was performed. On one of the samples, an additional annealing at 1000 and 1200 °C for 1 h was used. Raman/Photoluminescence (Raman/PL) measurements under optical laser excitation at 473 nm were performed in a non-confocal mode using a Raman spectrometer *Labram HR 800*. FTIR analysis [28] was performed in transmission at room temperature with a *Bruker Tensor 27 system*. Ultraviolet-Visible (UV-Vis) absorption spectra were acquired using a *Carry 6000i* spectrophotometer in the range 200-800 nm in a closed-cycle helium cryostat maintained at a temperature of 20-77 K. The absorption spectra have been normalized to the thickness of the CVD plates. More details on the experimental procedure can be found in [20]. And in order to access the spin properties and measure coherence times, ESR measurements were performed on two samples, one of which was annealed at 800°C and the other at 1200°C, by applying a microwave ramp (*Rohde & Schwartz SMB100A*) on a microwave antenna next to the sample and collecting the photoluminescence on an avalanche photodiode (*Thorlabs APD 130A*). The microwave amplitude was modulated at 900 Hz and the PL was

demodulated at the same frequency and filtered (*Standford Research System SR830*). The external magnetic field was applied with a homebuilt electromagnet or a permanent magnet [29].

3. Results and discussion

3.1. Effect of electron irradiation

The optical images of the 4 nitrogen-doped freestanding films presented in the first line of **Table 2** show that the growth conditions influence the colouration since they appear brown with a slight variation between them. Raman/PL analysis under 473 nm excitation was recorded after the different steps of the process. **Fig. 1**a shows the strong emission resulting from NV^0 and NV^- centres at 575 nm and 637 nm respectively as compared to the diamond Raman peak revealing that a relatively high amount of NV_s was successfully incorporated during CVD growth. We also confirm that, as already observed in a previous work [30], NV doping is clearly higher for the sample grown at lower temperature (sample A) while the other 3 samples grown at 1000 °C under different methane concentrations do not show any striking difference in PL. We finally note that, as expected for this excitation wavelength, NV^0 luminescence is preferentially excited as compared to NV^- while excitation at wavelength around 532 nm provide a more favourable excitation path for negatively charged NVs [31,32].

The effect of irradiation on PL spectra is illustrated in **Fig. 1**b. A broadband emission between 500 and 570 nm related to graphitization induced by high energy electron bombardment is observed. Besides this broadband, GR1 centres (neutral vacancies V^0 with a zero-phonon line (ZPL) at 741 nm) are observed indicating that vacancies were successfully created in the irradiated diamond plates. The creation of these defects clearly quenches NV emission which is much reduced after irradiation. This is consistent with the samples acquiring a dark-blue colour after irradiation as observed in the second line of **Table 2**.

	Sample A	Sample B	Sample C	Sample D
After growth			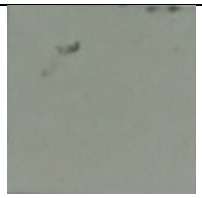	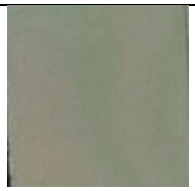
After e-irradiation	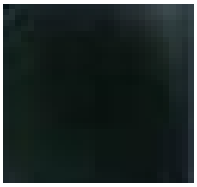			
After 800 °C annealing	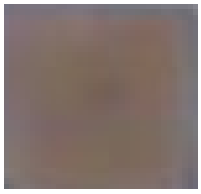	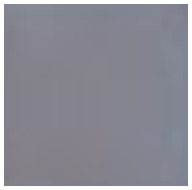	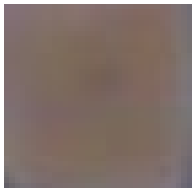	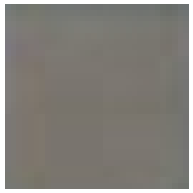

Table 2: Optical images of the four freestanding CVD films after each step.

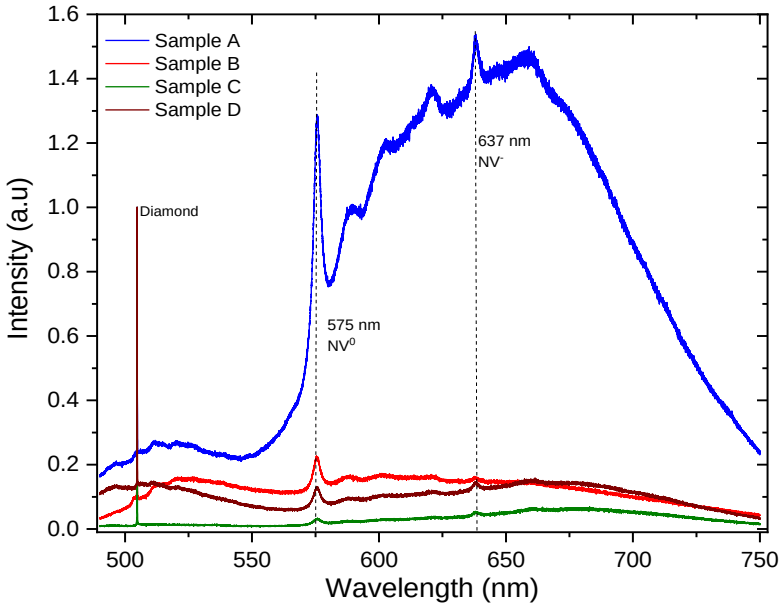

(a)

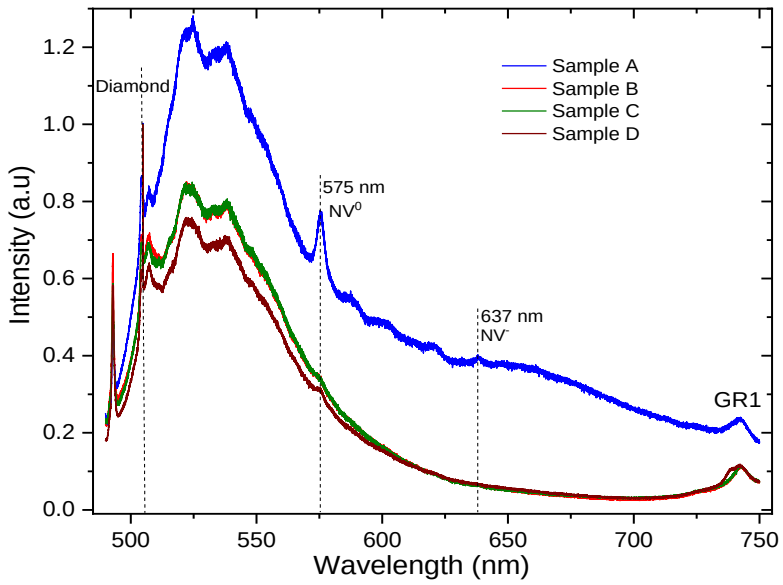

(b)

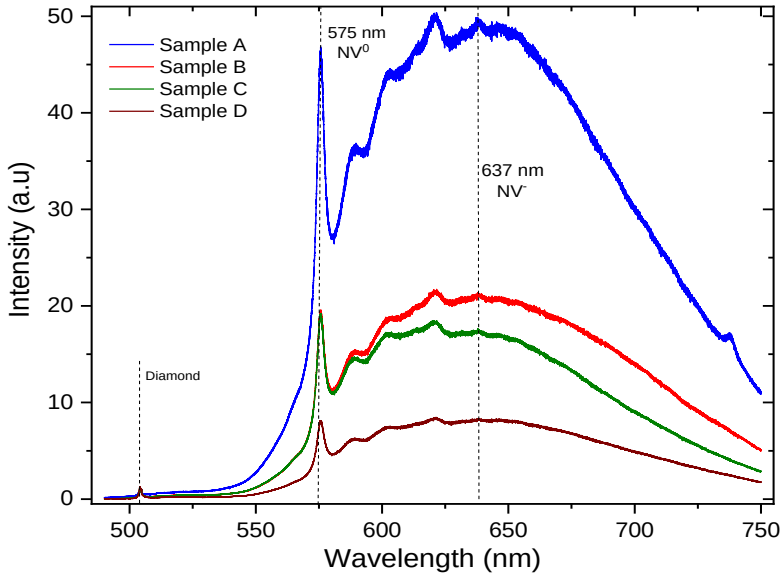

(c)

Fig 1. PL spectra normalized to the diamond Raman peak for different freestanding CVD diamond plates grown with N_2O addition: (a) as grown, (b) after electron irradiation and (c) after electron irradiation and annealing.

The PL spectra presented in **Fig. 1**c, illustrate the effect of thermal annealing. The graphite related component completely disappears, and the emission of NV centres strongly increases if we compare their intensity with the diamond Raman peak. This clearly indicates that created vacancies during irradiation moved towards nitrogen impurities and converted them into NV

centres. We note that as previously observed, the sample grown at lower temperature exhibits much stronger NV emission. In this sample too, we observe a weak component at 738 nm that comes from S_iV centres, a common background impurity in most CVD reactors.

3.2. Evaluation of defect concentration after the treatment

In order to evaluate the presence of other impurities in our CVD material, FTIR analysis was performed on the four samples after irradiation and thermal annealing and the corresponding spectra are presented in **Fig. 2**.

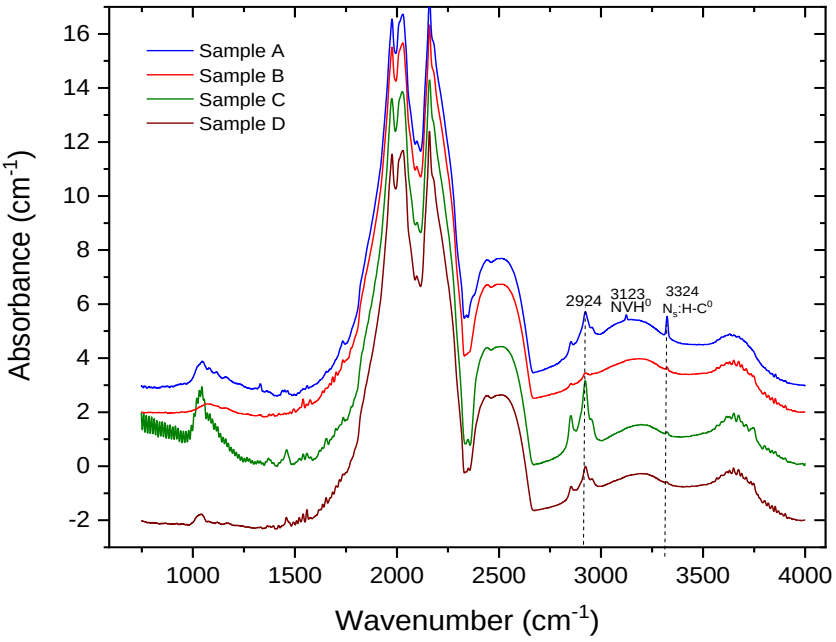

Fig 2. FTIR spectra of different freestanding CVD diamond plates grown with N_2O addition after electron irradiation and thermal annealing. The spectra were normalized to the 2-phonon absorption at around 2000 cm^{-1} and vertically shifted for clarity.

These spectra reveal the absence of large absorption bands in the one-phonon region (below 1332 cm^{-1}) induced by defects related to nitrogen. In particular, the bands usually present at 1130 cm^{-1} and 1332 cm^{-1} allowing estimating the amount of substitutional nitrogen in their neutral charge state (N_s^0) and in their positive charge state (N_s^+) respectively are under the detection limit (around 1 ppm) which confirms that electron irradiation followed by an annealing step is efficient to convert (at least partly) N_s to NV centres. The additional peaks observed between 2600 and 3400 cm^{-1} are related to hydrogen impurities. CH stretch corresponding to the peaks around 2900 cm^{-1} are evidenced as well as at 3123 cm^{-1} and

3324 cm^{-1} corresponding to NVH and N_s:H-C^0 (substitutional nitrogen decorated by an hydrogen atom) [20,33] respectively. It can be noted that these two specific defects are present more particularly when the sample was grown at lower temperature sample (sample A). H is a common impurity in CVD diamonds that are grown in a H_2-rich gas mixture. These defects thus probably appeared during growth.

Fig. 3 shows UV-Vis absorption spectra acquired at low temperature (20 K) for the 4 samples. Absorption due to NV centres with ZPLs at 637 nm and 575 nm and the absence of a clearly resolved absorption band at 270 nm (corresponding to electronic transitions from the valence band to N_s) confirm the results previously obtained with the FTIR measurements and the good conversion efficiency of N_s to NV centres after electronic irradiation and thermal annealing. An absorption band at 595 nm, likely due to radiation damage in nitrogen containing diamonds, is particularly visible after an annealing at 800 °C as previously reported by A. Zaitsev [34]. Another weak absorption peak at 723 nm, which has been reported in synthetic type Ib diamonds irradiated by high-energy electrons and subsequently annealed is also detected. It probably originates from defects created by the treatment and that were not completely annealed out.

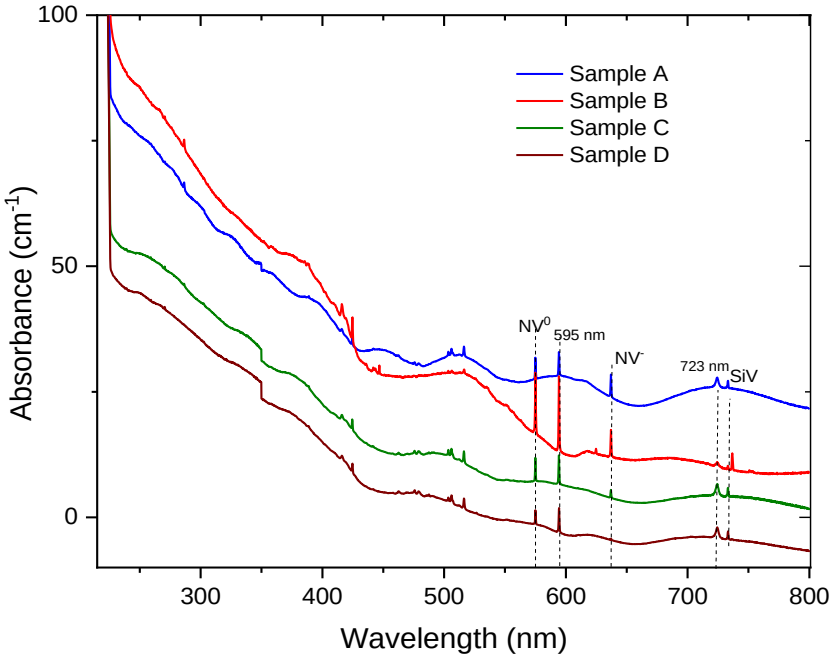

Fig 3. UV-visible optical absorption spectra at 20 K of the different freestanding CVD diamond plates grown with N_2O addition after electron irradiation and thermal annealing. Spectra are vertically shifted for clarity.

By integrating the areas of NV^0 and NV^- absorption peaks in the UV-Vis spectroscopy at a temperature of 77 K, we can estimate their concentration using the calibration constants given

in the literature [35]. This leads to a more reliable value than a direct extrapolation from PL intensity which is more prone to experimental artefacts due to power broadening or measurement conditions for example. The results obtained for the different samples are presented in **Table 3** and then plotted in Fig. 4. The total NV concentrations vary between 0.5 and more than 2 ppm depending on the growth conditions.

Samples	NV^- (ppb)	NV^0 (ppb)	NV_{Total} (ppb)	NV^-/NV_{Total} (%)
A	270	1900	2170	12
B	170	880	1050	16
B (an. 1000°C)	*130*	*751*	*881*	*15*
B (an. 1200°C)	*430*	*473*	*903*	*48*
C	430	1050	1480	29
D	40	520	560	7

Table 3: Calculated NV concentrations for the 4 CVD films irradiated and annealed at 800°C unless indicated otherwise

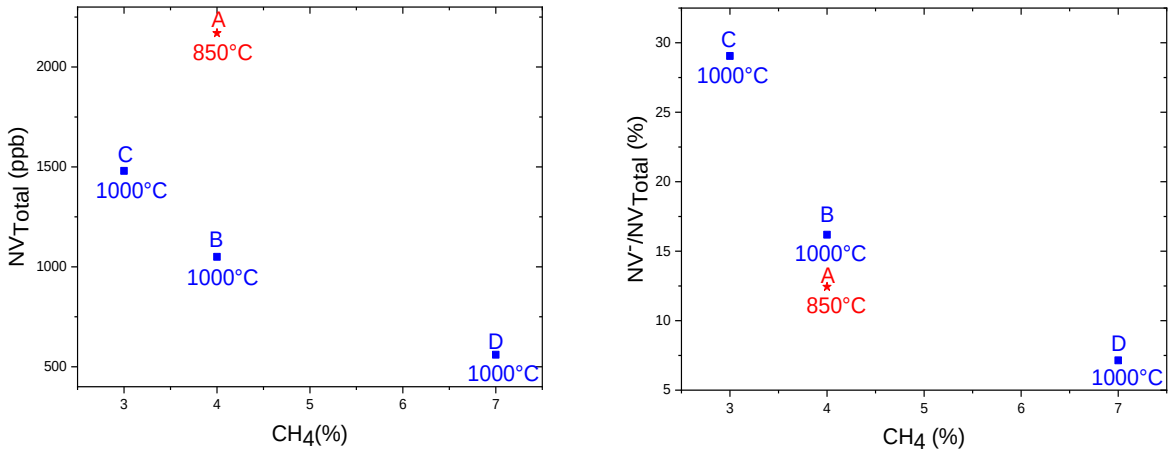

Fig 4. (a) Total NV concentration and (b) NV^-/NV^0 ratio evolution as a function of CH_4 for different growth temperatures (850°C or 1000°C) as indicated.

In Fig. 4a, a clear trend appears for the samples grown at the same temperature (in blue). The use of a lower methane concentration leads to a higher NV doping. In fact, one might have thought that the higher growth rates provided by an increased methane amount would have led to a higher incorporation of nitrogen impurities but that does not seem to be the case in our

growth conditions. To the contrary, as methane is decreased the probability of incorporating NVs in the films appears to be higher. We also confirm that a lower growth temperature strongly promotes the formation of NV centres for a given CH_4 concentration as previously observed [36]. Reducing deposition temperatures appears to enhance the trapping of nitrogen and more specifically vacancies in the film.

The evolution of NV^-/NV_{Total} ratio as a function of methane concentration is plotted in **Fig. 4b**. Again, we observe that lower methane concentration favours NV^- with respect to the total amount of NV incorporated. Reducing this parameter is thus favourable to quantum sensing applications in which higher NV^- densities are desired, although growth at low methane concentration comes at the expense of a reduced growth rate. Rather unexpectedly, a lower temperature increases the total amount of NV but does not seem very favourable to promote the negatively charged defect in this case. This possibly comes from the fact that, at low temperature, other defects are incorporated that might trap electrons and do not allow an easy charge transfer to NV centres.

In order to see whether other defects can be further removed, an additional annealing post treatment consisting in 1 hour at 1000°C and 1 hour at 1200°C was performed for sample B only. These two steps were followed by an acid cleaning treatment for 30 min at 200°C and O_2 plasma cleaning in order to remove the graphitic layer formed at the surface of the CVD diamond film. As illustrated in **Fig 5**, the 595 nm peak decreases after the first annealing at 1000°C and then totally disappears at 1200°C. The absorption spectrum becomes completely dominated by that of NV centres with almost no other remaining peaks. The results of NV concentration calculations are reported in Table 3. They show that while the total amount of NV is not significantly affected by the high-temperature annealing, the negative form of the NV centre seems to be favoured. This is consistent with a removal of charge trapping defects in this temperature range [37].

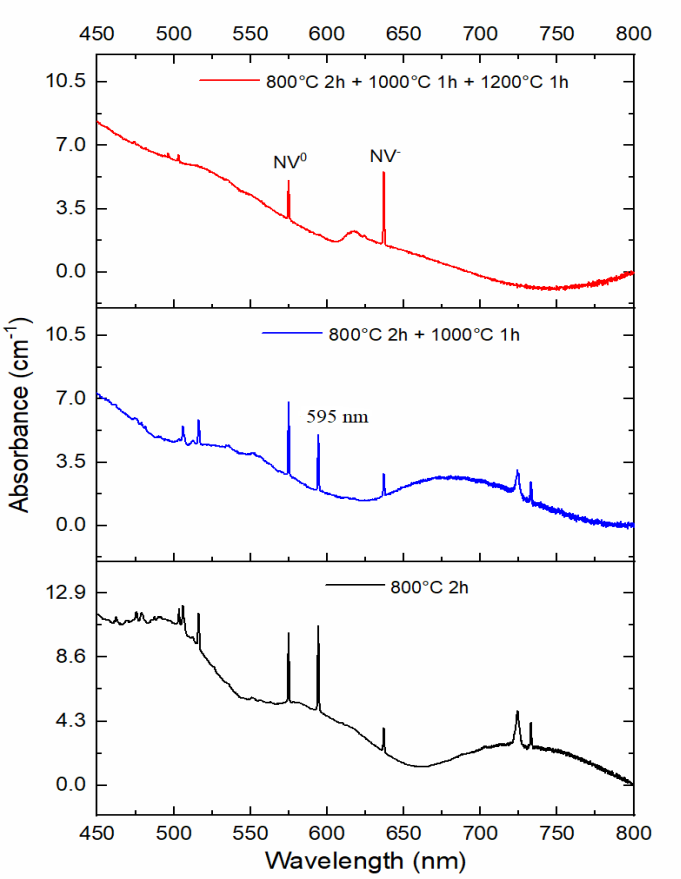

Fig 5. UV-Vis optical absorption spectra at 20 K of CVD diamond sample B grown with N_2O addition after electron irradiation and an increasing annealing temperature from 800 to 1200 °C.

3.3. Spin properties of NV ensembles

We eventually turn to ESR measurements in order to assess the spin properties of NV centres in our series of CVD diamond films. We took on these series two samples grown at the same temperature (1000°C) and which have had different annealing treatments at 800°C (Sample C) and 1200°C (Sample B). We first assessed the presence of defects by measuring NV^- photoluminescence while performing magnetic field scans in the 20 to 200 G range along the [100] crystalline axis to resonantly enhance dipole interactions and observe cross relaxations (CRs) and other spin impurities [29]. In **Fig. 6**a, two characteristic features appear at 50 G and 120 G for sample C (annealed at 800 °C only). They correspond respectively to the negative vacancy-hydrogen complex VH^- observed by Glover et al [38,39] and the War1 centre [40]. In contrast on the spectrum of the sample B (annealed at 1200°C), the VH^- contribution is absent while the War1 has decreased. Optically-detected ESR spectra of sample B and C are then

recorded for the two samples and reported in **Fig. 6b** and **c**. The PL is demodulated at the frequency of an alternating magnetic field and filtered to get a better signal and a Lorentzian fit is made. One can observe the typical ESR line with the characteristic hyperfine splitting due to interaction with ^{14}N leading to 3 peaks. It appears that for the sample annealed at higher temperature, a narrower linewidth is observed (0.390 against 0.582 MHz). This is consistent with the removal of defects, such as VH^-, as previously observed. Since the fits made here are Lorentzian, it is possible to get the half width at half height (HWHM). We can therefore use the convention given in [41] and find the values of the coherence time (T2*), which gives 408 ns for sample B and 273 ns for sample C. These values of T2* are consistent with a N_s^0 concentration of a few tens of ppm, as expected in these samples [41].

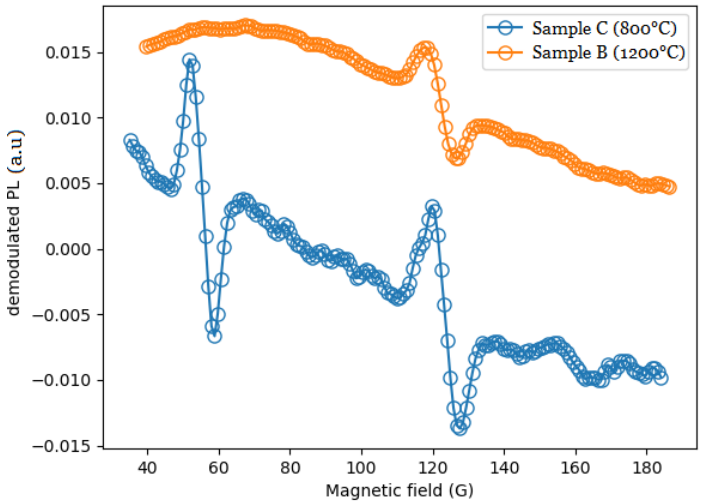

(a)

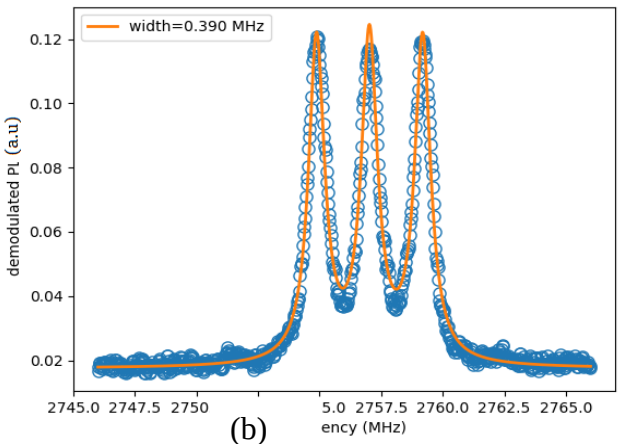

(b)

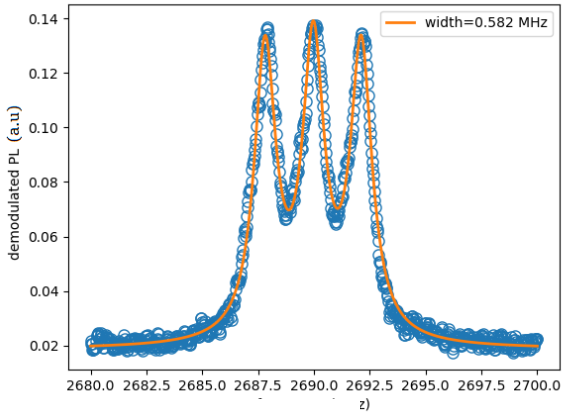

(c)

Fig 6. (a) PL as a function of magnetic field amplitude along the [100] crystalline axis. The spectra were vertically shifted for clarity. Optically-detected ESR spectra recorded by monitoring the NV defect PL intensity (b) for sample B (1200°C annealed) and (c) sample C (800°C annealed).

4. Conclusion

Obtaining high NV concentrations in CVD-grown diamonds is quite challenging but is a requisite for the development of sensitive quantum sensors that explore the coherent manipulation of the spin states of this atomic-scale defect. N_2O as a doping gas is particularly suited to preserve good crystal morphologies and to improve NV doping with good optical and spin properties. In this work we investigated different growth and annealing conditions of thick highly N-doped CVD diamonds allowing improving NV creation yield and properties. The samples were irradiated with high energy electrons (2.3 MeV) and annealed to convert substitutional nitrogen into NV. We successfully grew thick crystals with bright emission and NV content of the order of 0.5- 2 ppm. We concluded that the use of a lower methane concentration (< 4 %) and a lower temperature (850°C) both promote the incorporation of NV defects. However, a decrease of temperature was not so efficient at promoting the negatively charged state as a methane decrease, probably due to the incorporation of other types of defects. Annealing the crystals at 1200 °C after implantation was also successful to remove a great proportion of defects introduced by the irradiation treatment and led to a higher proportion of NV^- as well as improved spin properties. In particular, we evidenced that removal (or conversion) of VH^- defects was successful. The effect of growth and annealing conditions on the synthesis of thick NV-doped diamond crystals as reported in this work will guide efforts in engineering a diamond material that is suitable for quantum applications.

Acknowledgments

This work has received funding from the European Union's research and innovation program through the ASTERIQS project under grant agreement n° 820394, the Diamond-NMR project n° ANR-19-CE29-0017-04 and the Ile-de-France region in the framework of DIM SIRTEQ. ANR (Agence Nationale de la Recherche) and CGI (Commissariat à l'Investissement d'Avenir) are also gratefully acknowledged for their financial support through Labex SEAM (Science and Engineering for Advanced Materials and devices): ANR-10-LABX-096 and ANR-18-IDEX-0001. Grégory Lefevre from IRCP is thanked for his help with the FTIR analysis. Finally, we acknowledge the French EMIR-A (proposal N° 21-3033) network for the provision of irradiation beam time using the SIRIUS facility.

References:

[1] E.D. Herbschleb, H. Kato, Y. Maruyama, T. Danjo, T. Makino, S. Yamasaki, I. Ohki, K. Hayashi, H. Morishita, M. Fujiwara, N. Mizuochi, Ultra-long coherence times amongst room-temperature solid-state spins, Nat. Commun. 10 (2019) 3766. https://doi.org/10.1038/s41467-019-11776-8.

[2] M. Chipaux, A. Tallaire, J. Achard, S. Pezzagna, J. Meijer, V. Jacques, J.-F. Roch, T. Debuisschert, Magnetic imaging with an ensemble of nitrogen-vacancy centers in diamond, Eur. Phys. J. D. 69 (2015) 1–10.

[3] L. Rondin, J.-P. Tetienne, P. Spinicelli, C.D. Savio, K. Karrai, G. Dantelle, A. Thiaville, S. Rohart, J.-F. Roch, V. Jacques, Nanoscale magnetic field mapping with a single spin scanning probe magnetometer, ArXiv11084438 Cond-Mat. (2012). https://doi.org/10.1063/1.3703128.

[4] J.R. Maze, P.L. Stanwix, J.S. Hodges, S. Hong, J.M. Taylor, P. Cappellaro, L. Jiang, M.V.G. Dutt, E. Togan, A.S. Zibrov, A. Yacoby, R.L. Walsworth, M.D. Lukin, Nanoscale magnetic sensing with an individual electronic spin in diamond, Nature. 455 (2008) 644–647. https://doi.org/10.1038/nature07279.

[5] J.M. Taylor, P. Cappellaro, L. Childress, L. Jiang, D. Budker, P.R. Hemmer, A. Yacoby, R. Walsworth, M.D. Lukin, High-sensitivity diamond magnetometer with nanoscale resolution, Nat. Phys. 4 (2008) 810–816. https://doi.org/10.1038/nphys1075.

[6] V. Jacques, E. Wu, F. Grosshans, F. Treussart, P. Grangier, A. Aspect, J.-F. Roch, Experimental realization of Wheeler's delayed-choice GedankenExperiment, Science. 315 (2007) 966–968. https://doi.org/10.1126/science.1136303.

[7] A. Beveratos, R. Brouri, T. Gacoin, A. Villing, J.-P. Poizat, P. Grangier, Single Photon Quantum Cryptography, Phys. Rev. Lett. 89 (2002) 187901. https://doi.org/10.1103/PhysRevLett.89.187901.

[8] R. Brouri, A. Beveratos, J.-P. Poizat, P. Grangier, Photon antibunching in the fluorescence of individual color centers in diamond, Opt. Lett. 25 (2000) 1294. https://doi.org/10.1364/OL.25.001294.

[9] L.A. Stewart, Y. Zhai, J.M. Dawes, M.J. Steel, J.R. Rabeau, M.J. Withford, Single Photon Emission from Diamond nanocrystals in an Opal Photonic Crystal, Opt. Express. 17 (2009) 18044. https://doi.org/10.1364/OE.17.018044.

[10] C. Kurtsiefer, S. Mayer, P. Zarda, H. Weinfurter, Stable Solid-State Source of Single Photons, Phys. Rev. Lett. 85 (2000) 4.

[11] J.-R. Bertrand, C. Pioche-Durieu, J. Ayala, T. Petit, H.A. Girard, C.P. Malvy, E. Le Cam, F. Treussart, J.-C. Arnault, Plasma hydrogenated cationic detonation nanodiamonds efficiently deliver to human cells in culture functional siRNA targeting the Ewing sarcoma junction oncogene, Biomaterials. 45 (2015) 93–98. https://doi.org/10.1016/j.biomaterials.2014.12.007.

[12] M. Feng, I. D'Amico, P. Zanardi, F. Rossi, Spin-based quantum-information processing with semiconductor quantum dots and cavity QED, Phys. Rev. A. 67 (2003) 014306. https://doi.org/10.1103/PhysRevA.67.014306.

[13] M.A. Eriksson, M. Friesen, S.N. Coppersmith, R. Joynt, L.J. Klein, K. Slinker, P.M. Mooney, J.O. Chu, S.J. Koester, Spin-Based Quantum Dot Quantum Computing in Silicon, Quantum Inf. Process. (2004) 133–146. https://doi.org/10.1007/s11128-004-2224-z.

[14] N. Tsubouchi, M. Ogura, H. Kato, S.G. Ri, H. Watanabe, Y. Horino, H. Okushi, p-type doping by B ion implantation into diamond at elevated temperatures, Diam. Relat. Mater. 15 (2006) 157–159. https://doi.org/10.1016/j.diamond.2005.09.008.
[15] V.S. Vavilov, Ion implantation into diamond, Radiat. Eff. 37 (1978) 229–236.
[16] R. Kalish, C. Uzan-Saguy, B. Philosoph, V. Richter, J.P. Lagrange, E. Gheeraert, A. Deneuville, A.T. Collins, Nitrogen doping of diamond by ion implantation, Diam. Relat. Mater. 6 (1997) 516–520. https://doi.org/10.1016/S0925-9635(96)00657-7.
[17] A. Tallaire, A.T. Collins, D. Charles, J. Achard, R. Sussmann, A. Gicquel, M.E. Newton, A.M. Edmonds, R.J. Cruddace, Characterisation of high-quality thick single-crystal diamond grown by CVD with a low nitrogen addition, Diam. Relat. Mater. 15 (2006) 1700–1707. https://doi.org/10.1016/j.diamond.2006.02.005.
[18] M.L. Markham, J.M. Dodson, G.A. Scarsbrook, D.J. Twitchen, G. Balasubramanian, F. Jelezko, J. Wrachtrup, CVD diamond for spintronics, Diam. Relat. Mater. 20 (2011) 134–139. https://doi.org/10.1016/j.diamond.2010.11.016.
[19] J.J. Gracio, Q.H. Fan, J.C. Madaleno, Diamond growth by chemical vapour deposition, J. Phys. Appl. Phys. 43 (2010) 374017. https://doi.org/10.1088/0022-3727/43/37/374017.
[20] A. Tallaire, O. Brinza, P. Huillery, T. Delord, C. Pellet-Mary, R. Staacke, B. Abel, S. Pezzagna, J. Meijer, N. Touati, L. Binet, A. Ferrier, P. Goldner, G. Hetet, J. Achard, High NV density in a pink CVD diamond grown with N2O addition, Carbon. 170 (2020) 421–429. https://doi.org/10.1016/j.carbon.2020.08.048.
[21] J. Achard, F. Silva, O. Brinza, A. Tallaire, A. Gicquel, Coupled effect of nitrogen addition and surface temperature on the morphology and the kinetics of thick CVD diamond single crystals, Diam. Relat. Mater. 16 (2007) 685–689. https://doi.org/10.1016/j.diamond.2006.09.012.
[22] H. Koinuma, M. Yoshimoto, Y. Takagi, A.B. Sawaoka, T. HaHashimoto, T. Nagai, T. Shiraishi, Effect of Nitrous Oxide Gas on Cvd Diamond Film Deposition, MRS Proc. 180 (1990) 861. https://doi.org/10.1557/PROC-180-861.
[23] Y. Su, H.D. Li, S.H. Cheng, Q. Zhang, Q.L. Wang, X.Y. Lv, G.T. Zou, X.Q. Pei, J.G. Xie, Effect of N2O on high-rate homoepitaxial growth of CVD single crystal diamonds, J. Cryst. Growth. 351 (2012) 51–55. https://doi.org/10.1016/j.jcrysgro.2012.03.041.
[24] J. Achard, F. Silva, A. Tallaire, X. Bonnin, G. Lombardi, K. Hassouni, A. Gicquel, High quality MPACVD diamond single crystal growth: high microwave power density regime, J. Phys. Appl. Phys. 40 (2007) 6175–6188. https://doi.org/10.1088/0022-3727/40/20/S04.
[25] A. Tallaire, L. Mayer, O. Brinza, M.A. Pinault-Thaury, T. Debuisschert, J. Achard, Highly photostable NV centre ensembles in CVD diamond produced by using N_2O as the doping gas, Appl. Phys. Lett. 111 (2017) 143101. https://doi.org/10.1063/1.5004106.
[26] https://emira.ijclab.in2p3.fr/sirius/, (n.d.).
[27] B. Campbell, A. Mainwood, Radiation Damage of Diamond by Electron and Gamma Irradiation, Phys. Status Solidi A. 181 (2000) 99–107. https://doi.org/10.1002/1521-396X(200009)181.
[28] T.V. Martynova, N.I. Polushin, A.I. Laptev, A.L. Maslov, Express-analysis of nitrogen content in CVD-diamonds by FTIR-spectrometry, IOP Conf. Ser. Mater. Sci. Eng. 919 (2020) 022049. https://doi.org/10.1088/1757-899X/919/2/022049.
[29] C. Pellet-Mary, P. Huillery, M. Perdriat, A. Tallaire, G. Hétet, Optical detection of paramagnetic defects in diamond grown by chemical vapor deposition, Phys. Rev. B. 103 (2021) L100411. https://doi.org/10.1103/PhysRevB.103.L100411.
[30] A. Tallaire, J. Achard, A. Secroun, O. De Gryse, F. De Weerdt, J. Barjon, F. Silva, A. Gicquel, Multiple growth and characterization of thick diamond single crystals using

chemical vapour deposition working in pulsed mode, J. Cryst. Growth. 291 (2006) 533–539. https://doi.org/10.1016/j.jcrysgro.2006.03.046.
[31] N.B. Manson, M. Hedges, M.S.J. Barson, R. Ahlefeldt, M.W. Doherty, H. Abe, T. Ohshima, M.J. Sellars, NV^-–N^+ pair centre in 1b diamond, New J. Phys. 20 (2018) 113037. https://doi.org/10.1088/1367-2630/aaec58.
[32] N. Aslam, G. Waldherr, P. Neumann, F. Jelezko, J. Wrachtrup, Photo-induced ionization dynamics of the nitrogen vacancy defect in diamond investigated by single-shot charge state detection, New J. Phys. 15 (2013) 013064. https://doi.org/10.1088/1367-2630/15/1/013064.
[33] J.H.N. Loubser, J.A. van Wyk, Electron spin resonance in the study of diamond, Rep. Prog. Phys. 41 (1978) 1201–1248. https://doi.org/10.1088/0034-4885/41/8/002.
[34] A.M. Zaitsev, Optical Properties of Diamond, Springer. (2001) 519. https://doi.org/10.1007/978-3-662-04548-0.
[35] H. Hewitt, Colour centres on demand in diamond, Univ. Warwick. (2015) 250. http://webcat.warwick.ac.uk/record=b2870881~S1.
[36] A. Tallaire, M. Lesik, V. Jacques, S. Pezzagna, V. Mille, O. Brinza, J. Meijer, B. Abel, J.F. Roch, A. Gicquel, J. Achard, Temperature dependent creation of nitrogen-vacancy centers in single crystal CVD diamond layers, Diam. Relat. Mater. 51 (2015) 55–60.
[37] Boris Naydenov, Friedemann Reinhard, Anke Lämmle, V. Richter, Rafi Kalish, Ulrika F. S. D'Haenens-Johansson, Mark Newton, Fedor Jelezko, Jörg Wrachtrup, Increasing the coherence time of single electron spins in diamond by high temperature annealing, Appl. Phys. Lett. 97 (2010) 242511. https://doi.org/10.1063/1.3527975.
[38] C. Glover, M.E. Newton, P. Martineau, D.J. Twitchen, J.M. Baker, Hydrogen Incorporation in Diamond: The Nitrogen-Vacancy-Hydrogen Complex, Phys. Rev. Lett. 90 (2003) 185507. https://doi.org/10.1103/PhysRevLett.90.185507.
[39] C. Glover, M.E. Newton, P.M. Martineau, S. Quinn, D.J. Twitchen, Hydrogen Incorporation in Diamond: The Vacancy-Hydrogen Complex, Phys. Rev. Lett. 92 (2004) 135502. https://doi.org/10.1103/PhysRevLett.92.135502.
[40] R. Cruddace, Magnetic resonance and optical studies of point defects in single crystal CVD diamond, Univ. Warwick. (2007) 230.
[41] J.F. Barry, J.M. Schloss, E. Bauch, M.J. Turner, C.A. Hart, L.M. Pham, R.L. Walsworth, Sensitivity optimization for NV-diamond magnetometry, Rev. Mod. Phys. 92 (2020) 015004. https://doi.org/10.1103/RevModPhys.92.015004.